

Appendix 5

Viscous Damping in Various Configurations of HSX

A5.0 Introduction

As illustrated in Section 5.2 and Appendix 2, there are many different magnetic configurations accessible in HSX. Many of these configurations result in a breaking of the quasi-symmetry, as illustrated in the discussion of Hamada spectra in Section 5.2. This section provides examples of how these configurations differ with respect to the neoclassical viscous damping.

The appendix is divided into three subsections. The first section will present what might be considered the "smooth" radial profiles of viscous damping in the Mirror, antiMirror, Hill and Well configurations. "Smooth" in this sense implies that the local increase in viscous damping near magnetic islands will not be considered. The second section will consider the increase in viscous damping in the vicinity of magnetic islands for selected cases. The third section will briefly discuss the viscous damping in two configurations of HSX where the auxiliary coils have been configured to add spectral components with toroidal mode numbers greater than 4. Many more features of these configurations can be found in Section 5.2 and especially Appendix 2.

All calculations shown in this appendix are done using the full Hamada spectrum, calculated on at least seven well spaced magnetic surfaces to provide a radial profile. For computational efficiency, the large aspect ratio tokamak basis vectors are used when computing the flux surface averages of the magnetic field products (see Section 5.5). This approximation introduces small errors that can be neglected for these comparisons. The neutral density is set to zero in all calculations, so that the plots represent the damping due to symmetry breaking only. The inclusion of sufficiently many neutrals or another damping mechanism would work to obscure the neoclassical differences between the configurations.

Note that in all plots of neoclassical damping rates in this section, the effective minor radius r_{eff} is defined as $r_{\text{eff}}=100(\psi/\pi\cdot 0.5)^{1/2}$; the units of r_{eff} are cm. Here, ψ is the toroidal flux enclosed by the surface in Tm^2 and the field strength is always $B=0.5\text{T}$ on the magnetic axis at a toroidal angle of $\Phi=0$. Compared to a variable like r/a , this variable has the advantage of emphasizing the different sizes of the configurations.

A5.1: The "Smooth" Profiles of Viscous Damping in the Mirror, antiMirror, Well, and Hill Configurations.

The scaling of the three relevant time scales with respect to the Type 1 Mirror mode amp-turn percentage is shown in figure A5.1. The slow damping rate (γ_1) is most effected by the increasing amplitude of the $(n,m)=(4,0)$ mode amplitude, increasing by more than 2 orders of magnitude near the axis as the auxiliary coil amp-turn percentage is increased from 0 to 16%. The fast rate (γ_2) is changed by only a factor of two as the toroidal mirror term amplitude is increased. A tokamak analogy to this observation would be that the poloidal damping rate does not change if the modular coil ripple is increased. The time scale for the "Forced- E_r " model (ν_F) is seen to be intermediate to the two other time scales for all amp-turn percentages. It is impacted by the increasing symmetry breaking, but not as much as the slow rate.

A similar comparison is shown in figure A5.2 for the Type 1 antiMirror configurations. The antiMirror configuration has the current in the auxiliary coils going in the opposite direction compared to the Mirror configuration, leading to a 45 degree toroidal phase shift of the $(n,m)=(4,0)$ spectral component. This phase shift places a deep minima of $|B|$ at the toroidal angle of the ECH launcher. Experiments indicate that this deep ripple at the location of heating causes particles to drift out of the confinement volume; plasmas in the antiMirror configuration typically exhibit very low stored energy and reduced ECH power absorption compared to Mirror or QHS configuration plasmas.

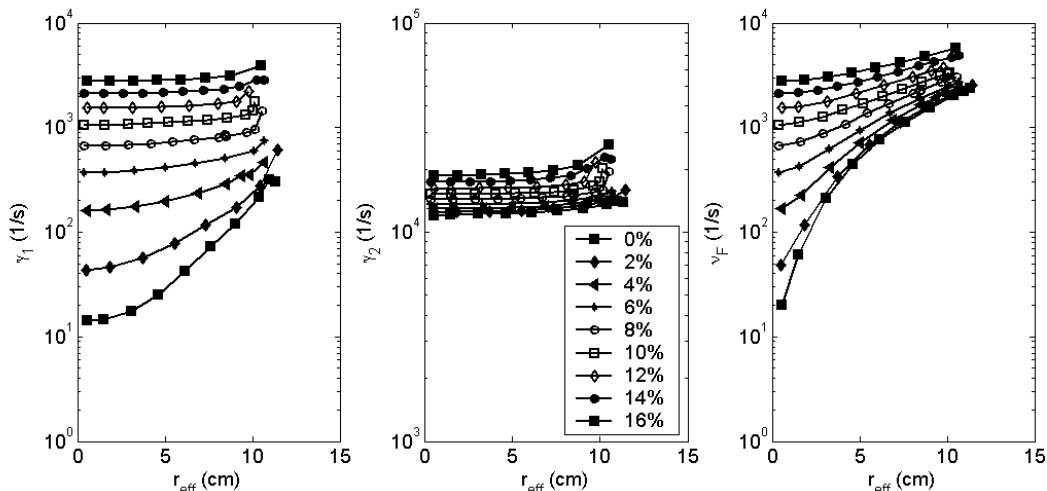


Figure A5.1: Profiles of the damping rates in the Type 1 Mirror configuration, with auxiliary coil current ranging from 0% to 16% of the amp-turns in the main coil set. Note the different scales.

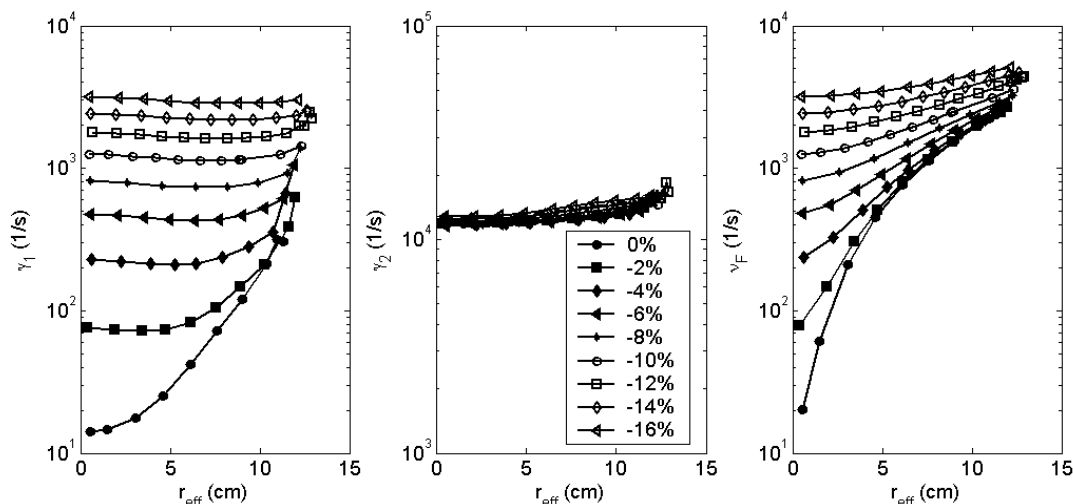


Figure A5.2: Profiles of the damping rates in the Type 1 antiMirror configuration, with auxiliary coil current ranging from 0% to 16% of the amp-turns in the main coil set. Note the different scales.

From the standpoint of viscous damping, the Mirror and antiMirror configurations are quite similar. Increasing the antiMirror amplitude induces strong changes in the slower damping rate, but leaves the faster damping rate largely unchanged. In this sense, the antiMirror configuration is globally similar to the Mirror.

The strong viscous damping trends in the Mirror and antiMirror configurations should be contrasted against the otherwise constant features of these configurations. As is shown in

Appendix 2, the Mirror configuration has a rotational transform that is slightly higher than the QHS configuration, while the antiMirror configuration has a rotational transform that is slightly smaller. Except at very high amp-turn fractions ($>14\%$), the well depth is not significantly changed in these configurations. The plasma volumes do not change by more than 20% in this range of configurations.

Viscous damping calculations in the Hill configuration are presented in figure A5.3. This configuration has a significant lowering of the rotational transform. At a Hill percentage between 5% and 5.25%, the $\iota=1$ surface enters the plasma in the core. Closed surfaces continue to exist outside of the $\iota=4/4$ island chain until the amp-turn percentage reaches $\approx 7\%$. The 6% Hill configuration has a very large $\iota=4/4$ island chain inside the separatrix, making it difficult to compare to configurations without this island chain. This configuration will be studied in more detail in Section A5.2.

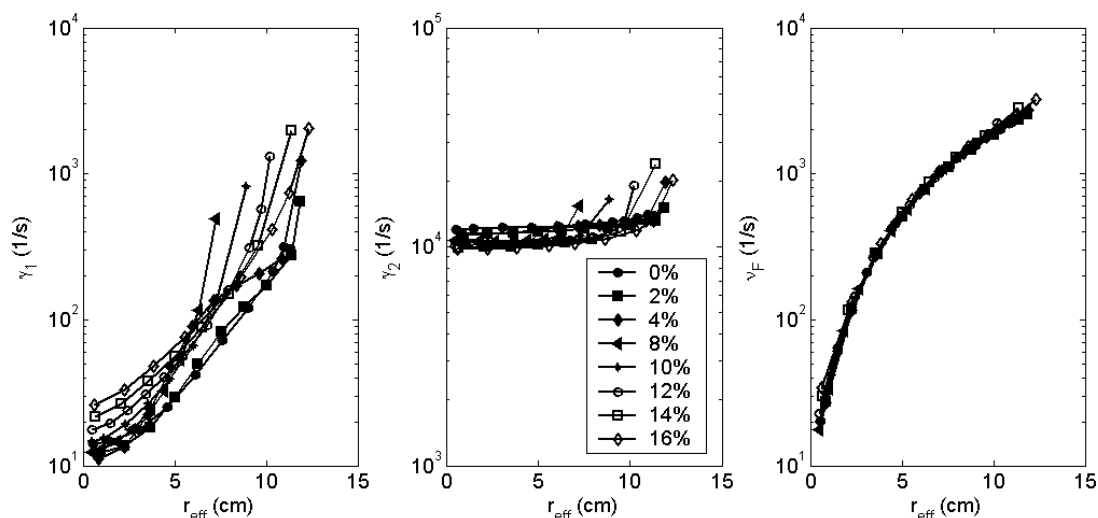


Figure A5.3: Profiles of the damping rates in the Hill configuration, with auxiliary coil current ranging from 0% to 16% of the amp-turns in the main coil set. Note the different scales.

There is a large different in the LCFS shape for configurations with edge rotational transform above or below 1. If the LCFS has $\iota > 1$, then the LCFS shape generally resembles that in the QHS. If the LCFS has $\iota < 1$, then the surface shape is generally more squared off (see

Appendix 2). These changes in shape will result in a breaking of the quasi-symmetry. This effect can be seen in the jump in viscous damping near the edge for configurations with $\iota(a) < 1$.

Viscous damping in the final standard configuration of HSX, the Well configuration, is shown in figure A5.4. This configuration results in a significant raising of the rotational transform, as well as a deepening of the magnetic well. As in the Hill configuration, the shape of the surfaces can change significantly, causing changes in the damping rates. Please refer to Appendix 2 for detailed information on the changes in the shape of the magnetic surfaces.

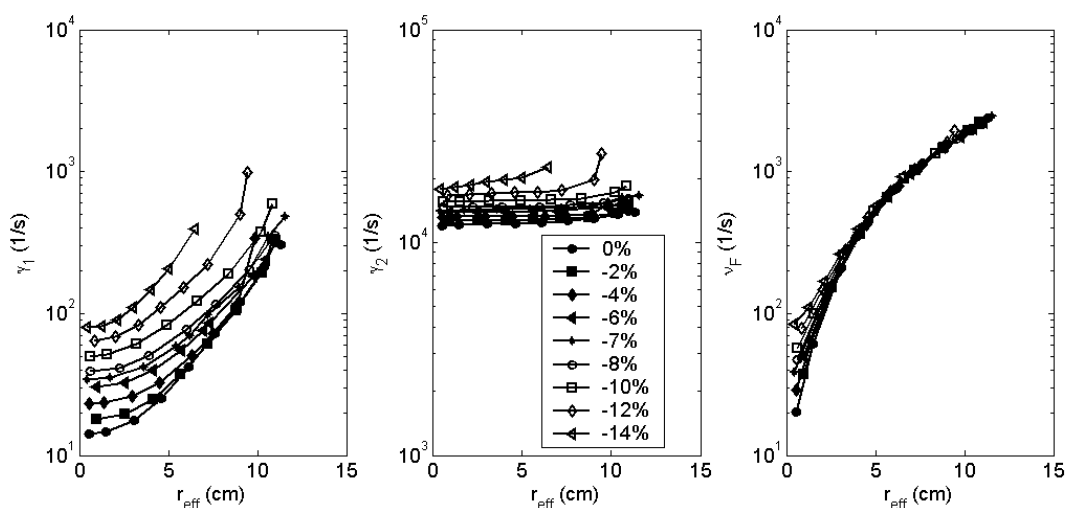


Figure A5.4: Profiles of the damping rates in the Well configuration, with auxiliary coil current ranging from 0% to 16% of the amp-turns in the main coil set. Note the different scales.

A5.2: Viscous Damping due to Magnetic Islands.

In addition to the viscous damping effects mentioned in the previous subsection, very interesting effects are seen in the vicinity of magnetic islands. These effects are the topic of this subsection, where four particular configurations of HSX will be considered. Other configurations of the HSX may also display similar features.

The rotational transform profiles for the four configurations studied in this section are presented in figure A5.5. Low order natural resonances are also shown as horizontal lines. There

is an $\iota=12/11$ surface present inside the last closed flux surface (LCFS) in the base QHS configuration. This resonance has been excluded in the 2% Hill configuration, where the auxiliary coils have been used to reduce the rotational transform. Continuing to reduce the rotational transform causes the $\iota=4/4$ surface to enter the plasma, at $\approx 5.25\%$ Hill. The rotational transform for the 6% Hill case is shown in the figure, illustrating the $\iota=4/4$ surface exists at approximately the half radius in this configuration. Also shown is the rotational transform for the 14% Mirror configuration. This configuration contains a large $(n,m)=(4,0)$ symmetry breaking spectral component across the entire plasma cross section. The rotational transform is also raised in this case, leading to an $\iota=8/7$ resonance inside the LCMS.

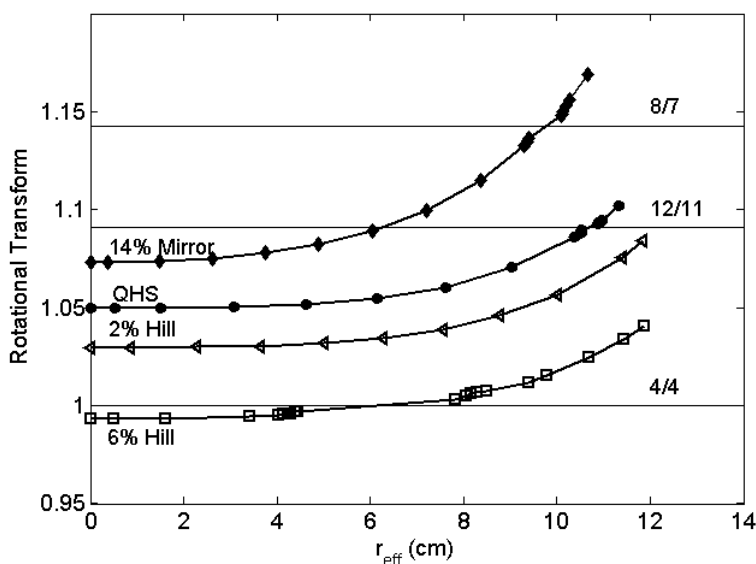


Figure A5.5: Rotational transform profiles for the four configurations under examination in this section. Various important low order rational surfaces are also displayed

The surfaces for the QHS, 6% Hill, and 14% Mirror configurations are shown in figure A5.6. The surfaces are vertical cuts at the approximately elliptical symmetry plane of HSX. Note that because HSX has a helical axis, yet the plots are made at fixed lab toroidal angle, these surfaces are slightly elongated compared to a view in the plane orthogonal to the magnetic axis. Each of the resonances noted in the previous paragraph is visible as an island chain. The

surfaces shown in the graphs are the surfaces on which Hamada spectrum and the damping calculations have been performed. The surfaces are carefully chosen so that regions of magnetic surfaces with fine structure are fully resolved.

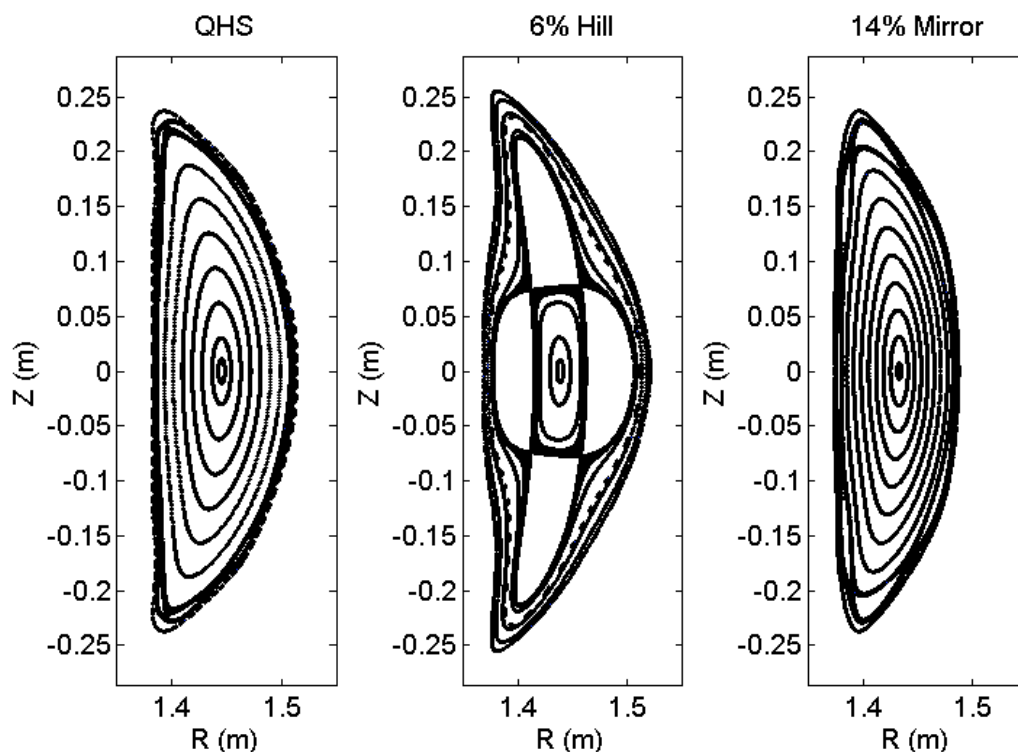


Figure A5.6: Magnetic surfaces in the QHS, 6% Hill, and 14% Mirror configurations. The islands are located in the gaps between surfaces.

The large $\iota=4/4$ island chain in the center frame of figure A5.6 illustrates most clearly the means by which the island chains break the quasi-symmetry. Near the axis, the surfaces have an elliptical shape which is similar to the shape in the QHS configuration. Near the inside of the island chain, the surfaces have developed a distinctly square shape. Crossing to the outside of the islands, the surfaces dive in toward the X-points. Moving toward the edge, the surfaces once again have a shape that is not dissimilar to the outer surface shape in the QHS configuration. Recall that these large deviations from the QHS surface shape are the result of a magnetic field perturbation at the level of 6% of the amp-turns of the main coil set. The volume inside the LCMS

for this 6% Hill configuration is $\approx 0.4 \text{ m}^3$. The volume enclosed by the square surface inside the island chain is $\approx 0.055 \text{ m}^3$ while the volume of the first closed surface outside of the island chain is $\approx 0.22 \text{ m}^3$. Hence, this island chain contains $\approx 40\%$ of the total volume inside the LCMS.

The Hamada spectra in configurations such as these were discussed in great detail in Section 5.2, and will not be discussed again. Instead, it is useful to assess complexity of the Hamada spectrum by plotting the total power in symmetry breaking spectral components for the different configurations. This quantity is defined as

$$\text{Power} = \left(\sum_{\substack{(n,m) \neq (0,0), (4,1) \\ n/4 \neq m}} b_{n,m}^2 \right)^{1/2}. \quad (\text{A5.1})$$

Note that this definition excludes the average field on a flux surface ($b_{0,0}$) and the main helical spectral component ($b_{4,1}$), as well as all spectral components with the same helicity as the $(n,m)=(4,1)$ component. This figure of merit is shown in figure A5.7 for the four configurations of interest.

The power in symmetry breaking components in the QHS configuration shows a general rise toward the edge, with a final level of about 2% at the LCMS. There is an increase in symmetry breaking power in the vicinity of the $\iota=12/11$ island, but it never exceeds the level at the LCMS. The Hill 2% case, where the $\iota=12/11$ island has been excluded, shows a monotonic rise of the symmetry breaking power toward the edge. The 14% Mirror case shows large symmetry breaking across the entire plasma cross section. This is due to the large $(n,m)=(4,0)$ spectral component introduced by the auxiliary coils. The effects of the $\iota=8/7$ island chain are not visible in this plot, but are instead obscured by the $(n,m)=(4,0)$ spectral component. The symmetry breaking impact of the $\iota=4/4$ island chain in the 6% Hill configuration is visible on either side of the island chain. Note that the QHS, 2% Hill, and 6% Hill configurations have very similar power in symmetry breaking spectral components in the center and at the LCMS, both of which locations are free of large scale island deformation in all three cases.

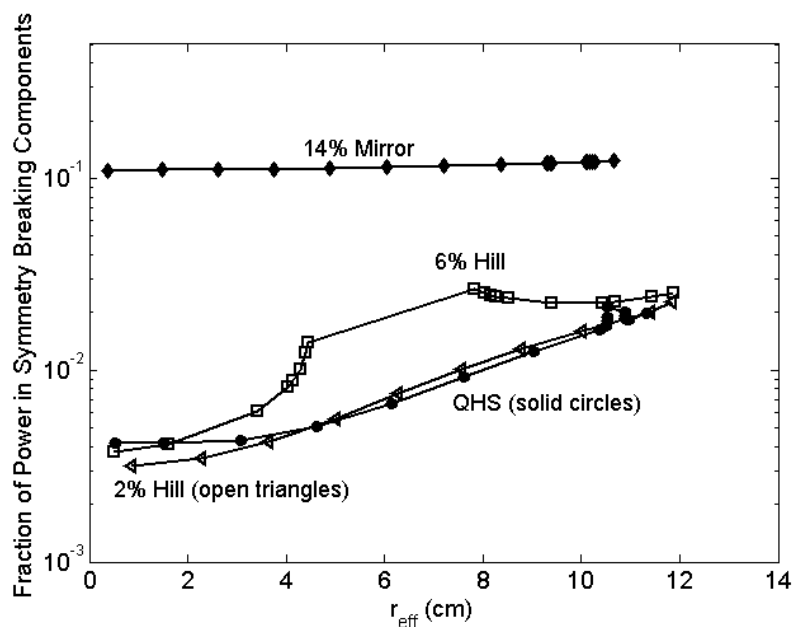


Figure A5.7: The total power in symmetry breaking spectral components for the four configurations under study in this subsection. The extra power due to the islands in the QHS and 6% Hill cases are visible, but the effects of the island are swamped by the $(n,m)=(4,0)$ spectral component in the 14% Mirror case.

With the detailed Hamada spectra information on surfaces near magnetic islands, it is possible to determine the viscous damping rates as described in Section 6.4. The plasma parameters are assumed to be the same in all calculations. A flat ion temperature profile with $T_i=20\text{eV}$ is used. A parabolic density profile is used with a small DC offset to provide some density at the edge. The profile is constrained to have a line average density of $1 \times 10^{12} \text{ cm}^{-3}$. The neutral density is set to zero in these calculations.

The slow damping rates for the four configurations are shown in top frame of figure A5.8. Recall that this rate corresponds to the damping of flows in the approximate direction of symmetry. The QHS and 2% Hill are very similar in this quantity, except for the increase in the damping in the vicinity of the $\iota=12/11$ magnetic island. The increase in the slow damping rate in the vicinity of the island is about a factor of 4 to 5. Note that the island has a width of 3mm effective minor radius out of a total minor effective radius of 11.3 cm, and that the effects of the

island die away within 0.5 mm on either side of the magnetic island chain. Furthermore, the fraction of the total volume enclosed inside these islands is only $\approx 6\%$ of the volume inside the LCMS. We infer for these reasons that the effects of this small island chain are not significant.

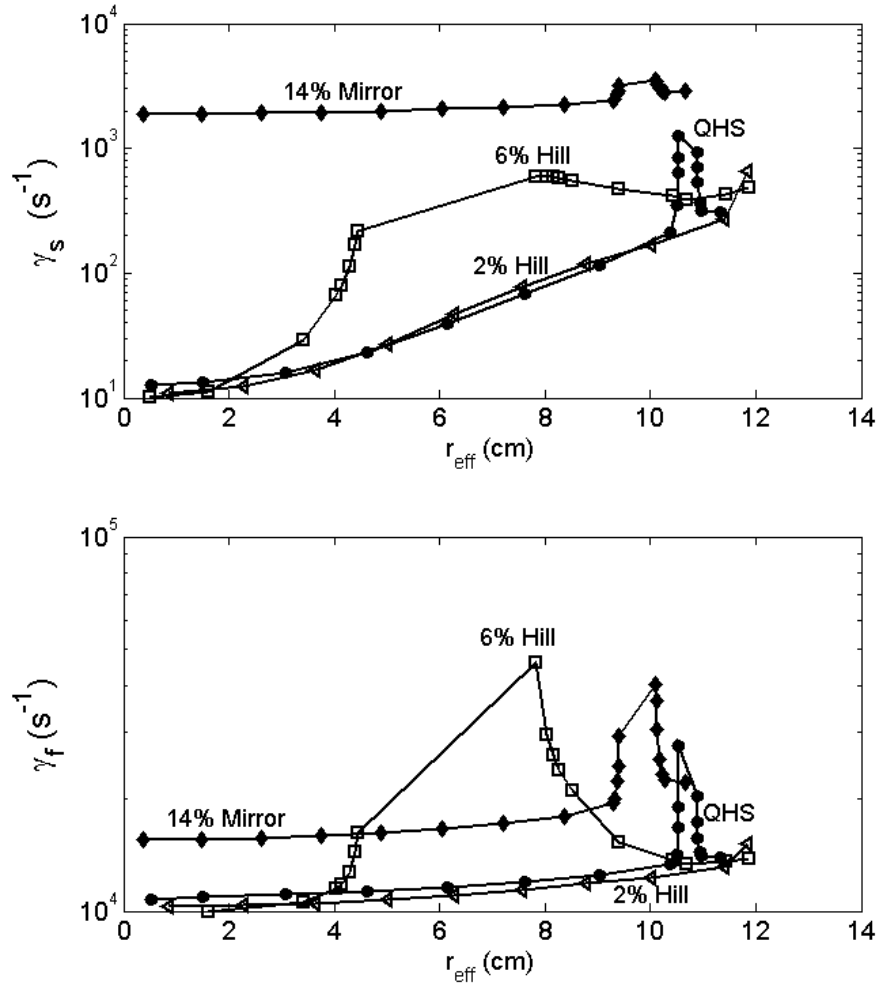


Figure A5.8: Slow damping rates (top) and fast damping rates (bottom) for the different configurations under consideration. There are peaks in the damping rates in the vicinity of the magnetic islands.

The damping due to this island in the QHS configuration can be compared to the large increase in damping across the entire minor radius in the 14% Mirror configuration. This configuration has a large $\iota=8/7$ island, whose effect is visible as only a factor of 2 perturbation to the already large slow damping rate. Once again, it is inferred that the effect of this island will be small. Had the quasi-symmetry not already been so badly broken by the Mirror spectral

component in this configuration, the effect of the $\iota=8/7$ island on the slow damping rate would have been more significant.

The most impressive island induced change in the slow damping rate is that in the 6% Hill configuration. On surfaces near the magnetic island, the increase in the viscous damping is quite large. On the other hand, both Hill configurations and the QHS configuration have comparable slow damping rates at the edge and near the center, where the impact of magnetic island surface distortions are minimal.

The fast damping rates are shown in the bottom frame of figure A5.8. Recall that this rate corresponds to the damping of flows across the direction of symmetry. Away from the islands, all four configurations have similar fast damping rates to within a factor of 2. In the vicinity of the magnetic islands the increase in the fast flow damping rate is quite large in all three configurations which contain an island chain. This increase in the fast rate due to the islands is apparently the dominant feature on the graph, and can overwhelm the differences in the neoclassical fast rate due to, for instance, the addition of the $(n,m)=(4,0)$ symmetry breaking components in the 14% Mirror configuration.

A5.3: Viscous Damping in Mirror Configurations With Toroidal Mode Number Greater than 4.

As a final calculation, the viscous damping in two exotic Mirror configurations of HSX has been studied. These configurations attempt to excite large mirror spectral components with toroidal mode numbers greater than 4. The so called Type 2 Mirror has alternating auxiliary coils reversing direction, while the Type 3 Mirror configuration has the auxiliary coils reversing sign after each pair of coils. More information on these configurations can be found in Appendix 2. The Hamada spectra for the 10% amp-turns case is shown in figure A5.9 and A5.10. The rotational transform profile is very similar to that in the QHS configuration, and the effects of islands are not considered in these calculations.

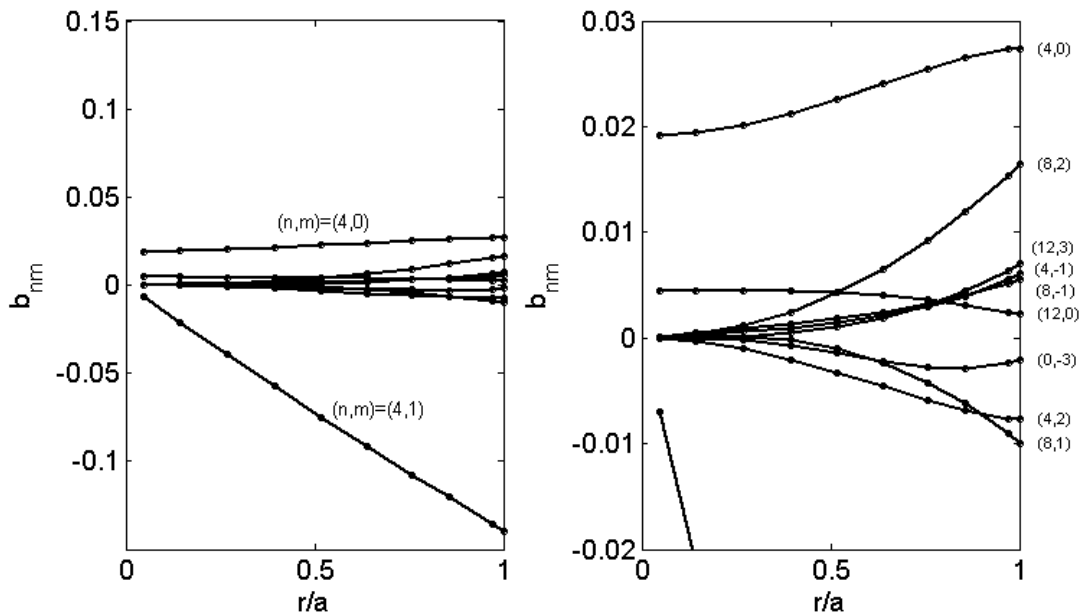


Figure A5.9: Hamada Spectra for the 10% Mirror Type 2 Configuration.

Inspection of these graphs reveals that higher toroidal mode number mirror spectral components, such as $(n,m)=(12,0)$, are indeed introduced into the spectrum. On the other hand their amplitude is significantly smaller than the $(n,m)=(4,0)$ component in the 10% Type 1 Mirror. With this point in mind, it is appropriate to compare the viscous damping in these configurations to the standard Mirror Type 1 configuration. These comparisons are done in figures A5.11 and A5.12. In each of these graphs, the damping rate at 10% Type 1 Mirror has been compared to the 10% and 20% amp-turn configurations of the Type 2 and 3 Mirror configurations.

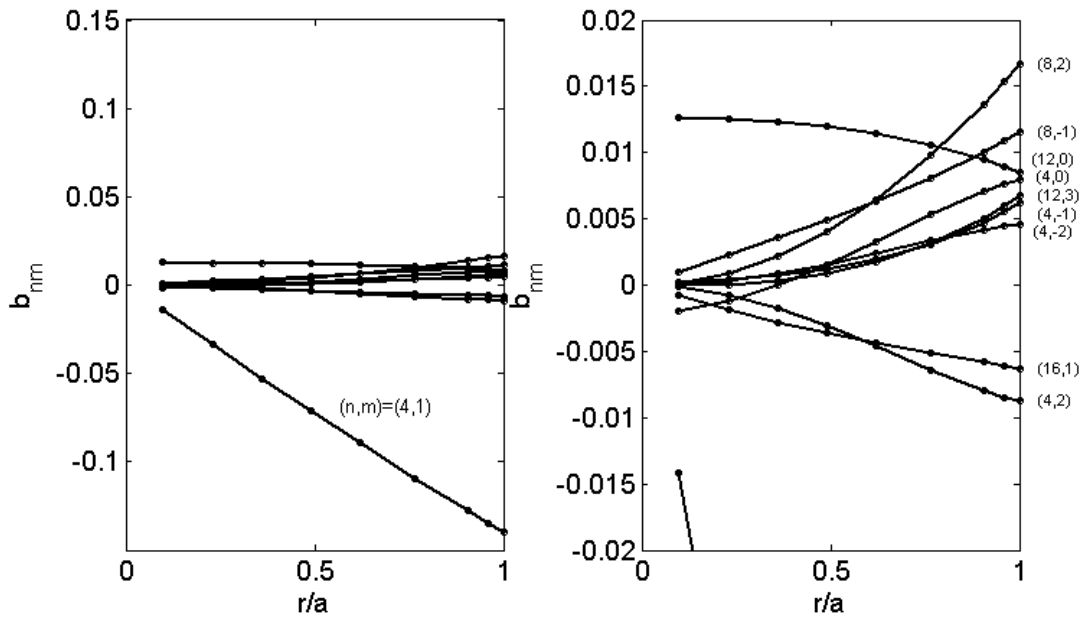


Figure A5.10: Hamada Spectra for the 10% Mirror Type 3 Configuration.

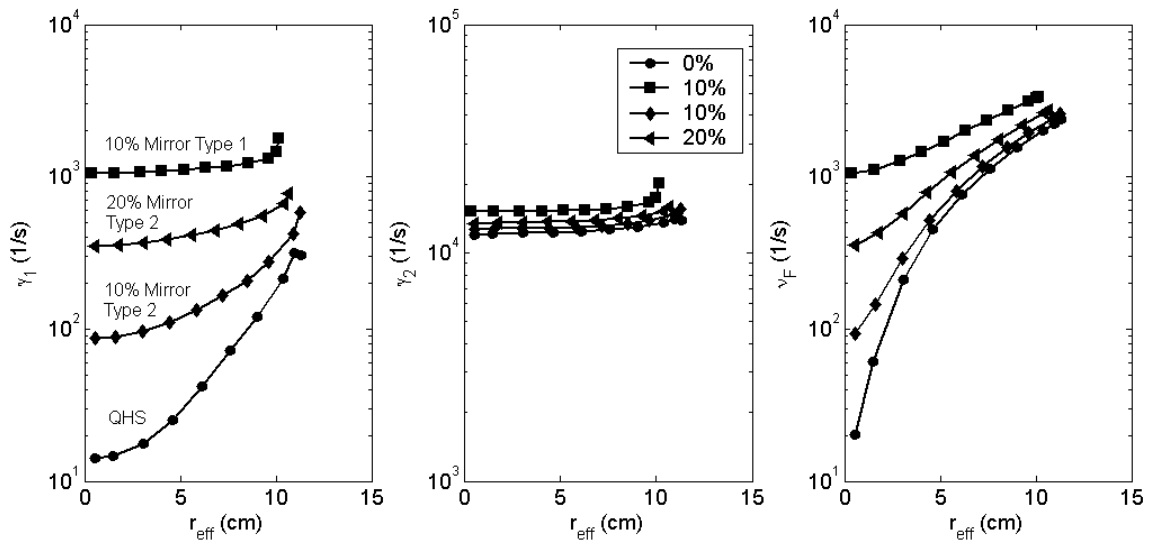


Figure A5.11: Comparison of the damping rates in the QHS, 10% Type 1 Mirror, and 10% and 20% Type 2 Mirror configurations.

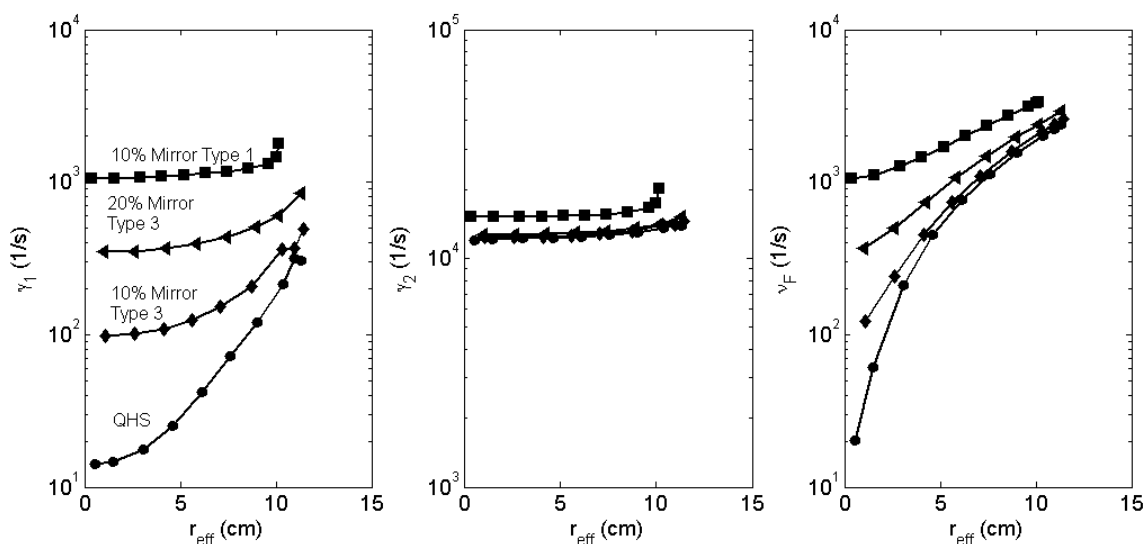


Figure A5.12: Comparison of the damping rates in the QHS, 10% Type 1 Mirror, and 10% and 20% Type 3 Mirror configurations.

It is immediately clear in these graphs that these configurations do not have as large an increase in viscous damping as the standard Type 1 Mirror, for fixed auxiliary coil current. Even at the 20% amp-turns level, the slow damping rate in either configuration is not as fast as that in the 10% Type 1 Mirror configuration. Given that these two configurations would require a significant amount of work rearranging auxiliary coil current feeds, it does not appear that they are worth the effort to study, at least from the standpoint of viscous flow damping.

A5.4: Summary

The neoclassical time scales have been compared for many different configurations of HSX. The standard Mirror and antiMirror configurations display a large increase in viscous damping. The Hill and Well configurations show smaller viscous damping increases. Mirror configurations designed to have perturbations with toroidal mode numbers >4 are not as efficient at increasing viscous damping as the standard Mirror configuration. This is mainly because the amplitude of the perturbations is smaller than in the standard Mirror configuration for a fixed auxiliary coil current.

Magnetic islands distort the shapes of surfaces surrounding them. This surface shape distortion causes a breaking of the quasi-symmetry, leading to an increase in the level of viscous damping. This increase is present near the $\iota=12/11$ resonance in the QHS configuration, but is much larger near, for instance, the $\iota=4/4$ resonance in the 6% Hill configuration.